Silicon (2021) 13:65–71
https://doi.org/10.1007/s12633-020-00407-3

ORIGINAL PAPER

Analysis of Double Gaussian Distribution at the Interface of Ni/Ta_2O_5/P-Si Schottky Barrier Diodes Using Temperature Dependent Current-Voltage (I-V) Measurements

Nallabala Nanda Kumar Reddy[1] · Chandramohan Kukkambakam[2] · V. Manjunath[3] · Vasudeva Reddy Minnam Reddy[4]

Received: 20 November 2019 / Accepted: 30 January 2020 / Published online: 11 February 2020
© Springer Nature B.V. 2020

Abstract
The electrical properties have been investigated for Ni/Ta_2O_5/p-Si Metal/insulator/semiconductor SBD in the temperature regime 175–400 K. The electrical parameters were analyzed using current-voltage characteristics as a function of operating temperature. It is observed that the Schottky barrier height increased whereas ideality factor and series resistance decreased with increasing the operating temperature. The characteristic temperature (T_o) value calculated from Norde and Cheung methods was compared. This analysis showed that T_o value extracted from both the techniques are in close agreement with each other. Experimental results revealed that the thermal coefficient was −4.5 mV/K. The Gaussian distribution of the barrier height was estimated from the plot of zero-bias barrier height (Φ_{bo}) versus 1/2kT plot and the estimated value of (Φ_{bo}) of 0.92 eV and 0.79 eV with standard deviation (σ_0) of 0.023 V and 0.014 V, respectively. The mean BH and the Richardson constant values were determined using ln (I_o/T^2)-$q^2\sigma_0^2$ /2$(kT)^2$ versus 1000/T plot and were 0.89 eV and 0.76 eV and 30.03 and 26.85 A/cm^{-2} K^{-2}, respectively. In addition to the thermionic emission process, two more conduction mechanisms such as Poole-Frenkel emission in the temperature regime 175–275 K and Schottky emission dominant beyond 300 K temperature were noticed.

Keywords MIS Schottky barrier diode · Series resistance · Ta2O5 dielectric layer · Double Gausssian Disribution

1 Introduction

Presently, the development of semiconductor devices in nano-scale regime creates a huge demand for the study of high-k dielectric materials as they became the prime constituents in almost all Si-based devices [1, 2]. The reduction of SiO_2 high-k insulating layer thickness less than few nanometers is susceptible to direct tunneling of electrons causing a severe leakage current issue in devices fabricated on Si semiconductor [3]. Thus, various high-k materials such as HfO_2, ZrO_2, Y_2O_3, La_2O_3, CeO_2 and Ta_2O_5 are presently under consideration to replace the conventional SiO_2 layer due to the above said limiting factors. Among these high-k dielectrics, tantalum pentoxide (Ta_2O_5) appear to be the most capable material owing to its higher dielectric constant, tolerable breakdown voltage, reasonably low leakage currents and thermal/chemical stability at higher temperatures [4, 5]. Due to these outstanding characteristic properties, Ta_2O_5 found applications such as coatings [6], high storage capacitors [7], electrochromic devices [8] and catalysts [9]. Previously, various research groups have utilized RF sputtering [9], sol-gel [10] and pulsed laser deposition [11] to deposit the Ta_2O_5 films onto various substrates.

The deposition of metal film onto silicon semiconductor surface is acknowledged as metal-semiconductor (MS) contacts/Schottky barrier diodes (SBDs) which is very simple and plays a significant key role in all most all semiconductor based electronic devices such as integrated circuits, optoelectronics and devices functioning in the microwave region [12]. The performance of these devices for instance device

✉ Nallabala Nanda Kumar Reddy
nandasvu@gmail.com

✉ Vasudeva Reddy Minnam Reddy
drmvasudr9@gmail.com

[1] Department of Physics, Madanapalle Institute of Technology and Science, Madanapalle, A.P 517325, India

[2] Department of Chemistry, Madanapalle Institute of Technology and Science, Madanapalle, A.P 517325, India

[3] Department of Physics, Sri Padmavati Mahila Visvavidyalayam, Tirupati, A.P 517 501, India

[4] School of Chemical Engineering, Yeungnam University, Gyeongsan 38541, Republic of Korea

reliability and stability can be biased by the interface properties of the barrier created between the semiconductor and metal. In majority of the realistic MS contacts, even a special care has been taken during the fabrication process always a thin native oxide layer will be present on the semiconductors surface which is inevitable [13]. The presence of this unintentionally formed oxide layer translates the above said MS structure into a metal-insulator-semiconductor (MIS) type heterostructures with remarkable modifications in the electronic parameters of the fabricated device [14]. The performance of these MIS type SDs specifically depends on the formation of the interfacial oxide layer, interface between metal and semiconductor, distribution of interface states that prevail on the semiconductor surface, series resistance and inhomogeneous BHs [15]. In addition, the rectifying characteristics of these MIS type heterostructure SDs are assessed by means of the significant parameters such as Schottky barrier height (SBH), series resistance (R_S) and ideality factor (n) values extracted from current-voltage (I-V) characteristics. Extraction of these rectifying characteristic parameters for the MIS type SBDs from I-V characteristics alone at room temperature may possibly not adequate to explain the current transport mechanisms and the nature of the barrier formation at the interfaces of the prepared heterojunction [16–18].

Already it is familiar that the temperature has a significant impact on the performance of the above said MIS type SBD devices. Fabrication and development of high performance heterojunction based SD devices working below and above room temperature is necessary to reveal the type of current transport processes taking place at the interface between the metal and semiconductor [16, 17]. In this manuscript, we employed Ta_2O_5 as an insulating oxide layer and fabricated Ni/Ta_2O_5/p-Si MIS type heterojunction using electron beam evaporation technique. Thus, to reveal the type of current transport mechanisms other than TE that is taking place at the MIS interface, for the first time we extended our analysis on temperature dependent electrical parameters of MIS type SBDs with Ta_2O_5 as an interfacial oxide layer onto p-type Silicon in the temperature regime 175–400 K.

2 Experimental Details

In this work, we used boron doped p-type Si <100> wafer with a resistivity of ~5–10 Ωcm for the fabrication of the proposed MIS type Schottky diode heterostructure. Before metal deposition, the native oxides were removed from the surface of the p-Si semiconductor pieces using the cleaning procedure steps as mentioned in our previous report [19]. Subsequently, the samples were rinsed in deionized water and then blown with high purity N_2 gas. Then, the samples were loaded into the vacuum chamber of the 3 kW e-beam evaporation system. When the attained pressure inside the chamber was below 2.5×10^{-5} mbar, aluminium (150 nm) was deposited on the rough surface of the p-Si wafer by e-beam evaporation system. To make the deposited Al metal as a better Ohmic contact to p-Si, these samples were subjected to annealing process at 450 °C for 5 min in high purity N_2 gas. Firstly, tantalum pentoxide (Ta_2O_5) film of thickness 30 nm is deposited on the entire smooth surface of the p-Si wafer piece and consequently, Ni metal film of thickness 40 nm is deposited on the top of the Ta_2O_5 film deposited on p-type Si using physical mask which consists of 1 mm diameter circular gaps. The thickness measurements are performed using Quartz crystal monitor (Model:CTM-200) and during the deposition the pressure inside the vacuum chamber was observed to be varied from 3.3×10^{-5} mbar to 4×10^{-5} mbar. The I-V chracteristics of the fabricated as-deposited Ni/Ta_2O_5/p-Si/Al type MIS structures were measured as a function of operating temperature using Keithley 2400 Source meter in association with liquid nitrogen cryostat arrangement.

3 Results and Discussion

We analyzed the experimental current-voltage-temperature (I-V-T) characteristics of Ni/Ta_2O_5/p-Si MIS SBD in the temperature regime 175–400 K and are shown in Fig. 1. We tried to measure the I-V-T characteristics from 70 K. But, the current transport mechanism has been started/taken place from the operating temperature of 175 K. It is noticed that the leakage current increased from 1.93×10^{-10} A (at 175 K) to 2.149×10^{-5} A (at 400 K) with an increase in temperature at -1 V. The calculated turn on voltage ($V_{turn\text{-}on}$) values of the fabricated MIS SBD at the current of -1 μA (at -1 V) is depicted in Fig. 2. The $V_{turn\text{-}on}$ was noticed to be decreased from 1.12 V at 175 K to 0.11 V at 400 K.

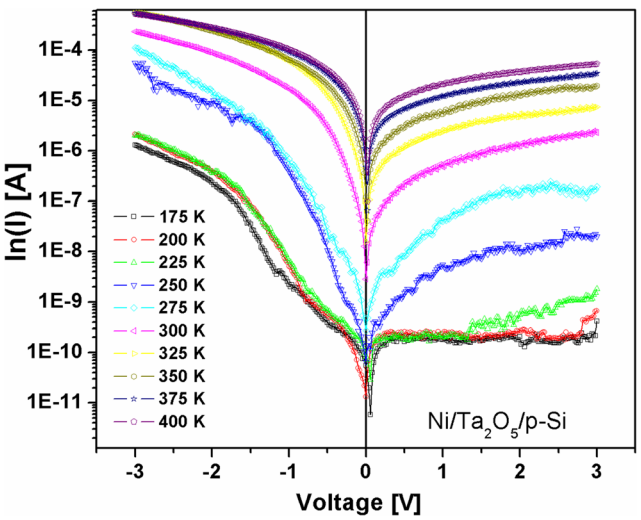

Fig. 1 Experimental reverse and forward bias current-voltage (I-V) characteristics of Ni/Ta_2O_5/p-Si SBD in the temperature regime 175–400 K

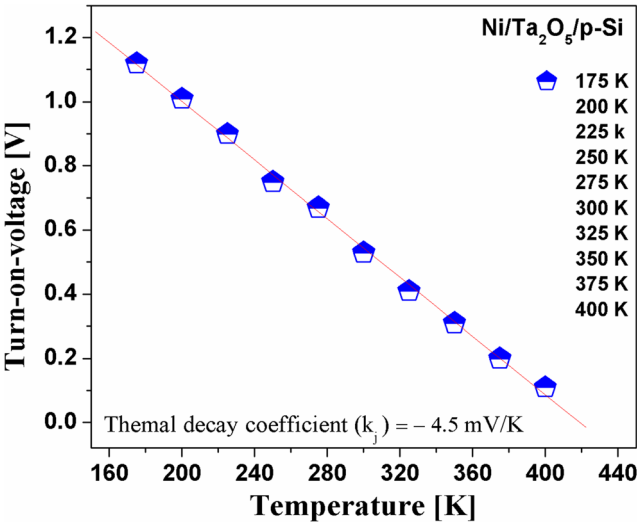

Fig. 2 Experimental $V_{turn\text{-}on}$ for the $Ni/Ta_2O_5/p\text{-}Si$ MIS SBD. The straight line indicates the best fittings with the theoretically obtained data using Eq. (1)

The coefficient of thermal decay (K_j) was evaluated from the plot of $V_{turn\text{-}on}$ versus temperature by numerical fitting to the experimentally obtained I-V characteristics of MIS SBDs (Fig. 1) using the following equation [20–24].

$$Kj = -\frac{\Delta V_{turn-on}}{\Delta T} = \left[\frac{q\left(V_{turn-on}-E_g\right)}{qT} + \frac{1}{q}\frac{dE_g}{dT} - \frac{3k_B}{q}\right] \quad (1)$$

Where 'E_g' is band gap energy, $V_{turn\text{-}on}$ is turn-on voltage and k_B is Boltzmann's constant. The above equation resembles the fundamental temperature dependence of the $V_{turn\text{-}on}$. Also, the first, second and third parts of eq. (1) corresponds to temperature dependence of carrier concentration, band-gap energy and effective density of states (EDS), respectively. Calculations revealed that the EDS exhibiting minute temperature-dependence, resulting drop in $V_{turn\text{-}on}$ value. The reason for this observed trend was ascribed to the reduced bandgap energy and enhancement of carrier concentration of the semiconductor. From numerical fitting of the attained results, the K_j for the fabricated $Ni/Ta_2O_5/p\text{-}Si$ MIS SBD in the present study is found to be −4.5 mV/K and is in close agreement with the previous reports [24].

The observed nonlinearity in the forward bias ln(I)-V plot in higher voltage regime as in Fig. 1 for $Ni/Ta_2O_5/p\text{-}Si$ MIS SBD is attributable to the series resistance (R_S) and interface state density (N_{SS}) that prevailed at the two interfaces exists in the prepared device structure. The R_S of the fabricated MIS structure is equivalent to the summation of total resistance value of the resistors connected in series and resistance at the semiconductors junction in the current flow direction. As evident from Fig. 1, the I-V curves of the $Ni/Ta_2O_5/p\text{-}Si$ MIS SBD exhibited good rectification. Accordingly, we evaluated the 'R_S', 'Φ_b' and 'n' values for the prepared $Ni/Ta_2O_5/p\text{-}Si$ MIS SBD by employing the Cheung equation [20–23, 25–27].

$$\frac{dV}{dIn(I)} = IR_S + \frac{nk_BT}{q} \quad (2)$$

and

$$H(I) = V - \frac{nk_BT}{q}\ln\left(\frac{I_o}{AA^*T^2}\right) = n\Phi_{bo} + IR_S. \quad (3)$$

The experimentally obtained 'R_S' versus 'T' for $Ni/Ta_2O_5/p\text{-}Si$ SD is shown in Fig. 3. From Fig. 3, the 'R_S' and 'n' values of the $Ni/Ta_2O_5/p\text{-}Si$ MIS SBD were found to be 3976 Ω and 3.62 at 175 K and 469 Ω and 1.26 at 400 K, respectively. These findings signify that the 'R_S' values and the resultant 'n' were found to decrease with the increase in operating temperature and these values were tabulated in Table 1. Using exponential decay relation $R_S \propto \exp.(-T/T_o)$, a plot of '$R_S$' versus 'T' was constructed and the characteristic temperature (T_o) value was estimated as 77.51 K from Cheung's function. From Fig. 4, the 'R_S' and 'Φ_b' values of $Ni/Ta_2O_5/p\text{-}Si$ MIS structure were estimated as 4153 Ω and 0.50 eV at 175 K and 381 Ω and 0.84 eV at 400 K, respectively. The 'R_S' values were exponentially decreased whereas the 'Φ_b' values were increased and the extracted 'T_o' value was estimated as 82.75 K from Cheung's function. These observed temperature dependence of 'n', 'R_S' and 'Φ_b' was ascribed to the intentionally deposited Ta_2O_5 interfacial oxide layer/inhomogeneity in thickness and interface states that present between the deposited metal and p-Si [28, 29]. Also, the current transport process at the metal-semiconductor (MS) interface is stimulated by the diodes operating temperature. Hence, the carriers easily surmount the lower barriers patches at low temperatures resulting in larger ideality factor. At higher operating temperatures, more and more carries accomplishes the necessary thermal energy which is adequate to overcome the

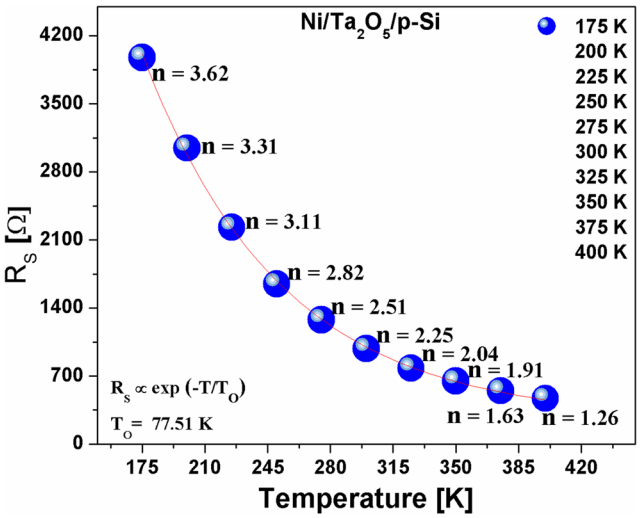

Fig. 3 Temperature dependence plots of the experimentally obtained R_S and n for the $Ni/Ta_2O_5/p\text{-}Si$ MIS SBD using Cheung functions. The solid line shows the theoretical values estimated from the numerical fittings using the equation:[$R_S \propto \exp.(-T/T_o)$]

Table 1 R_S, n and Φ_{bo} calculated for the fabricated Ni/Ta_2O_5/P-Si MIS SBDs in the temperature regime 175–400 K

Temperature (K)	Idealityfactor (n)	Series resistance (Rs) (Ω)			Barrier heights (Φ_b) eV		
		dV/dlnI vs. I	H(I) vs. I	Norde Method	I-V	Cheung	Norde
175	3.62	4153	3976	7493	0.49	0.50	0.52
200	3.31	3168	3043	5114	0.58	0.61	0.63
225	3.11	2354	2230	3406	0.65	0.65	0.67
250	2.82	1770	1646	2121	0.72	0.73	0.75
275	2.51	1277	1277	1470	0.76	0.77	0.79
300	2.25	929	982	1136	0.78	0.79	0.81
325	2.04	710	780	893	0.80	0.81	0.83
350	1.91	594	648	748	0.81	0.82	0.84
375	1.63	477	548	595	0.82	0.82	0.85
400	1.26	381	469	468	0.83	0.84	0.86

higher barrier patches yielding the increase in effective SBH. The variations of ideality factor and SBH as a function of temperature evidently confirm that the current conduction process deviates from pure TE theory due to presence of R_S in the fabricated device. On the other hand, the effect of the image force, structural defects in the semiconductor, inhomogeneous doping, interface roughness, interfacial reactions, tunneling and recombination-generation process may also enhance the ideality factor value from one [26, 29, 34].

To calculate the reliable SBH and R_S value for the fabricated Ni/Ta_2O_5/p-Si MIS SBD, we employed Norde method. This Norde's function can be represent as [30].

$$F(V) = \frac{V}{2} - \frac{KT}{q}\ln\left[\frac{I}{AA^{*}T^{2}}\right] \tag{4}$$

Here 'I' indicates the obtained current from basic I-V plot. The minimum of the F (V) versus V plot is determined and then the 'Φ_b' values can be evaluated from eq. (5), where $F(V_{min})$ is the minimum value of F (V) and V_{min} is the consequent voltage

$$\Phi_b = F(V_{min}) + \frac{V_{min}}{2} - \frac{k_B T}{q} \tag{5}$$

The SBH values calculated using the above equation (Norde method) by plotting F(V) versus V plot is shown in Fig. 5 and the values were tabulated in Table 1. The R_S values can be evaluated from the Norde method using the equation

$$R_S = \left[\frac{k_B T}{q I_{min}}(2-n)\right] \tag{6}$$

where, I_{min} is minimum current corresponding to the minimum voltage (V_{min}). According to the equation $R_S \propto \exp(-T/T_o)$, i.e., the exponential decay relationship between R_S and T, the 'T_o' was calculated as 56.43 K (from Fig. 6). The calculated R_S values were found to decrease exponentially and corresponding Φ_b

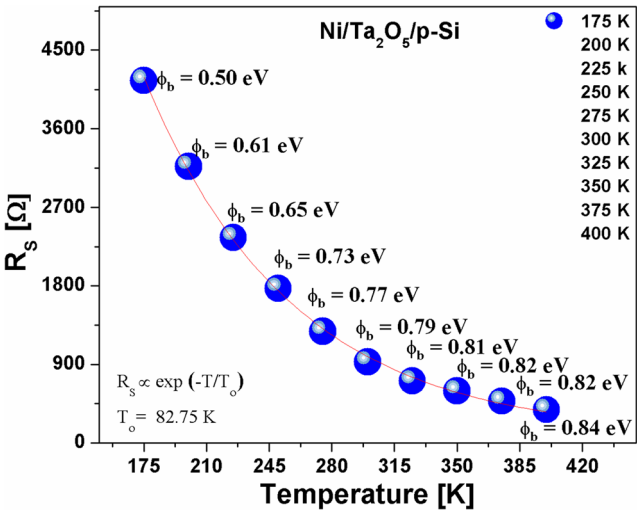

Fig. 4 Plots of temperature dependence of R_S and Φ_b for the Ni/Ta_2O_5/p-Si SBD in the temperature regime 175–400 K using Cheung function. The solid line shows the theoretical values obtained from the numerical fitting using the equation:[$R_S \propto \exp.(-T/T_o)$]

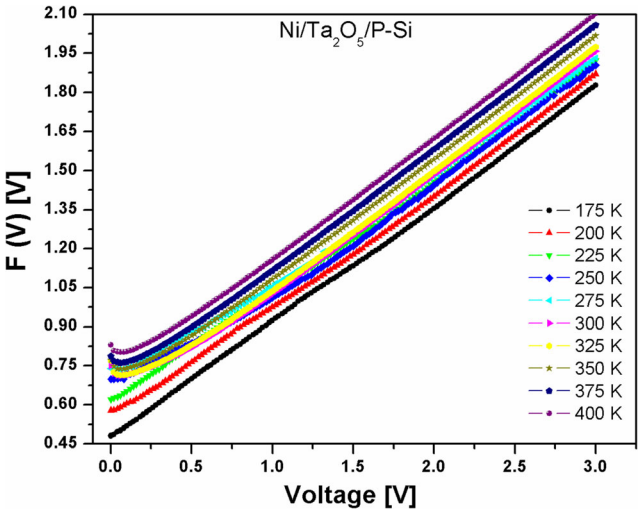

Fig. 5 F(V) versus V curves for Ni/Ta_2O_5/p-Si SBD in the temperature regime 175–400 K

increased considerably with increase in temperature. Similar trends were observed in previous works [31, 32]. In addition from the Table 1, it is observed that the value of R_S obtained from Norde function is higher than those obtained from Cheung function. This is due to the fact that Cheung function are only applied to the nonlinear region in high voltage segment of the forward-bias ln(I)-V characteristics, while the Norde model might be suitable method especially for the lower voltage regime of the forward bias I-V characteristics of the rectifying junctions, which are non-agreed with pure thermionic emission (TE) theory. As a result, R_s value extracted from Norde functions could be much higher than the Cheung model for especially non-ideal rectifying structures [33]. The SBH, R_S and ideality factors extracted from various methods as a function of temperature were compared and depicted in Fig. 7.

Assuming the Gaussian distribution (GD) of the barrier heights (BHs) with a mean SBH value ($\overline{\Phi}_b$) and standard deviation (σ_o), the apparent barrier height Φ_{ap} and ideality factor n_{ap} were calculated according to the following equations [31, 34].

$$\Phi_{ap} = \overline{\Phi}_b\ (\mathrm{T} = 0\ \mathrm{K}) - \frac{q\sigma_0^2}{2k_B T}. \tag{7}$$

$$\left(\frac{1}{n_{ap}} - 1\right) = \rho_2 - \frac{q\rho_3}{2k_B T}. \tag{8}$$

$\overline{\Phi}_b$ and $\sigma_o$are linearly bias dependent on Gaussian parameters such as $\overline{\Phi}_b = \overline{\Phi}_{bo} + \rho_2 V$ and standard deviation as

$$\sigma_s^2 = \sigma_{so+}^2 \rho_3 \mathrm{V} \tag{9}$$

where ρ_2 and ρ_3 are voltage coefficients which significantly depends on operating temperature and they assess the voltage deformation of BH distribution. Moreover, the temperature dependence of $\sigma_s$is usually small and can be neglected [17, 18]. To investigate the evidence of a GD of the SBH in the vicinity of the metal and semiconductor, the plot of Φ_{ap} versus 1/2kT was plotted and is shown in Fig. 8. In general, it should be a single straight line which can provide $\overline{\Phi}_{bo}$ and σ_o from the intercept and slope values, respectively. But in this work, two straight lines were employed to fit the evaluated experimental data. The determined $\overline{\Phi}_{bo}$ and σ_o values from the two straight line fittings were 0.92 eV and 0.023 V in the temperature regime 300–400 K (region-II) and 0.79 eV and 0.014 V in the temperature regime 175–275 K (region-I), respectively. Likewise, the plot of $(1/n_{ap})$ versus 1/2kT gives two straight lines from which the voltage coefficients ρ_2 and ρ_3 were calculated by utilizing the intercept and slope values, respectively. The resulting values of $\rho_2 = 0.39$ V and $\rho_3 = 0.047$ V in 175–275 K regime (region-I) and $\rho_2 = 0.28$ V and $\rho_3 = 0.014$ in 300–400 K regime (region-II). Similar trend of double GD of BH were observed in previous works [34, 35].

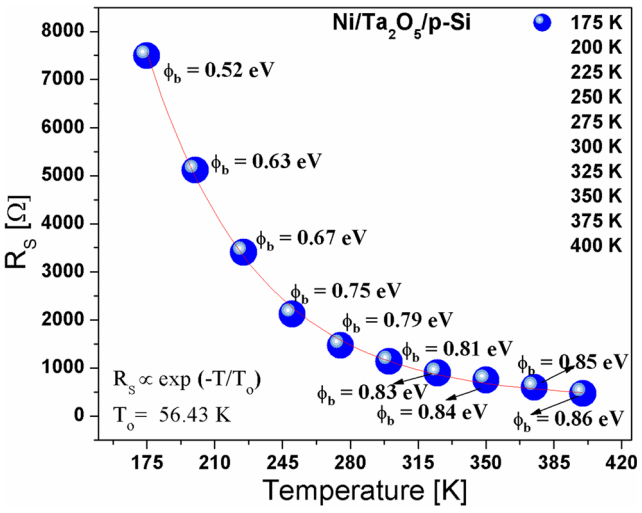

Fig. 6 Plots of temperature dependence R_S and Φ_b for the Ni/Ta_2O_5/p-Si SBD in the temperature regime 175–400 K using Norde function. The solid lines shows the theoretical values obtained from the numerical fitting using the equation: [$R_S \propto \exp.(-T/T_o)$].

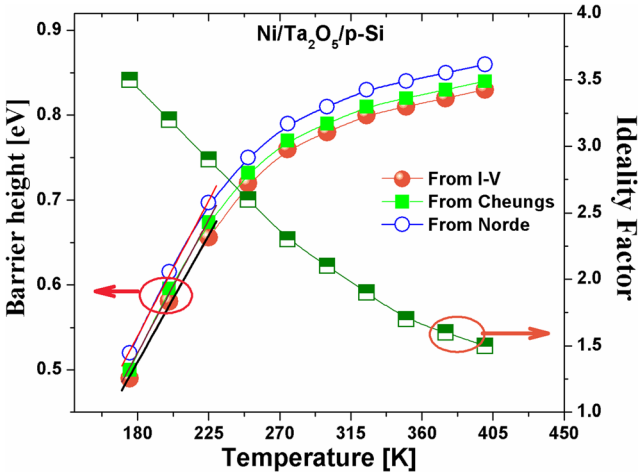

Fig. 7 The SBH and ideality factor versus temperature plot for Ni/Ta_2O_5/p-Si SBD in the temperature regime 175–400 K

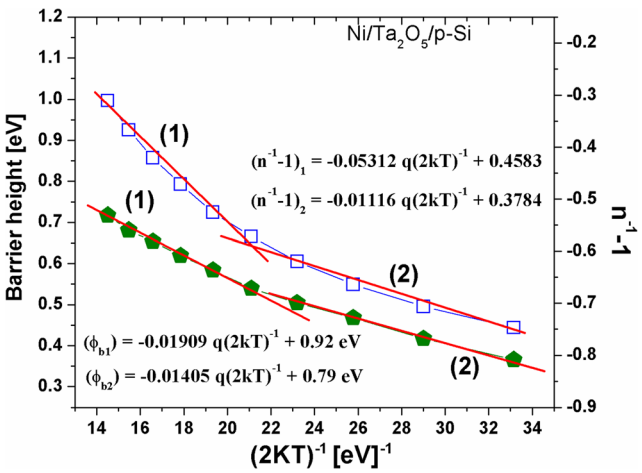

Fig. 8 The zero-bias apparent barrier height and ideality factor versus 1/2kT plot for the Ni/Ta_2O_5/p-Si SBD according to double GD of BHs

This represents that the ideality factor does in fact conveys the voltage deformation of the GD of the SBH. These observations suggest that the inhomogenities exists at the barrier and fluctuations in potential notably influence the I-V characteristics that were measured at low temperatures for the prepared Ni/Ta_2O_5/p-Si MIS SBDs.

In general, the conventional Richardson plot (not shown here) exhibits non-linearity on the basis of TE mechanism [33, 34]. Thus, by considering the equations $I_o = AA^*T^2\exp(-q\Phi_{bo}/KT)$ and $\Phi_{ap}=\overline{\Phi}_{bo}$ (T = 0 K)-$(q\sigma_0^2/2kT)$, the modified Richardson plot can be expressed according to the GD BHs as.

$$\ln\left(\frac{I_0}{T^2}\right)-\left(\frac{q^2\sigma_0^2}{2k_B{}^2T^2}\right) = \ln(AA^*)\frac{q\overline{\Phi}_b}{k_BT} \tag{10}$$

Figure 9 represents the modified Richardson plot of $\ln(I_o/T^2)$-$q^2\sigma_o^2$ /2 K^2 T^2 versus 1000/T and should provide a straight line with the slope and intercept values yielding the mean barrier height ($\overline{\Phi}_{bo}$) and A^*. The fittings were made to two linear portions with a transition occurring at 275 K. The estimated values of $\overline{\Phi}_b$ and A* were found to be 0.76 eV and 26.85 Acm^{-2} K^{-2} in 175-275 K temperature regime and 0.89 eV and 30.03 Acm^{-2} K^{-2} in 300–400 K temperature regime. Thus, the estimated Φ_{bo} values from this plot are in excellent agreement with the Φ_b values extracted from Fig. 8. The calculated values of A* from both the temperature regimes are in close agreement with the theoretical value of 32.6 Acm^{-2} K^{-2} for p-Si [36].

As the calculated ideality factor values are exceeding more than one (Fig. 7) at all measured temperatures ranging from 175 to 400 K, notify that the probable current transport process at the interface of Ni/Ta_2O_5/p-Si MIS SBDs is not only limited to TE mechanism. As a result, to classify the main current transport mechanisms such as Poole-Frenkel emission (PFE) [37] and Schottky emission (SE) that takes place at the interface of the fabricated Ni/Ta_2O_5/p-Si MIS SBDs, we utilized reverse-bias I-V characteristics. This was made possible by plotting a graph between reverse current ($\ln(I_R)$) and its corresponding voltage ($(V_R)^{1/2}$) and is illustrated in Fig. 10. Generally, the current in PFE can be expressed as

$$I_R = I_o\exp\left(\frac{\beta_{PFE}V^{1/2}}{k_BTd^{1/2}}\right) \tag{11}$$

where as the dominant current in SE process can be expressed as

$$I_R = AA^{**}T^2\left(\frac{-\Phi_b}{k_BT}\right)\exp\left(\frac{\beta_{SE}V^{1/2}}{k_BTd^{1/2}}\right) \tag{12}$$

where, β_{PFE} and β_{SE} are the PFE and SE field lowering coefficients, respectively. And the theoretical values of β_{SE} and β_{FE} are calculated by the following equation [38].

$$2\beta_{SE} = \beta_{PFE} = \left(\frac{q^3}{\pi\varepsilon_0\varepsilon_s}\right)^{1/2} \tag{13}$$

Using the above equation, the field lowering coefficient's theoretical values and experimental slope values for Ni/Ta_2O_5/p-Si MIS SBDs for different temperature is shown in Fig. 10. Here, the calculated theoretical values of these coefficients for the Ni/Ta_2O_5/p-Si MIS SBDs were $\beta_{PE} = 2.461\times10^{-4}$ $eV/m^{1/2}V^{1/2}$ and $\beta_{SE} = 1.230\times10^{-4}$ $eV/m^{1/2}V^{1/2}$. The experimental slopes values extracted from linear fit to the experimental data of MIS junction are depicted in Fig. 10 and were 2.091×10^{-4}, 2.197×10^{-4}, 2.165×10^{-4}, 2.154×10^{-4}, 2.153×10^{-4}, 1.971×10^{-4}, 1.925×10^{-4}, 1.900×10^{-4}, 1.897×10^{-4}, and 1.883×10^{-4} $eV/m^{1/2}V^{1/2}$ for temperatures 175, 200, 225, 250, 275, 300, 325, 350, 375 and 400 K respectively. Comparison of the experimental and theoretical values of Ni/Ta_2O_5/p-Si MIS SBD revealed

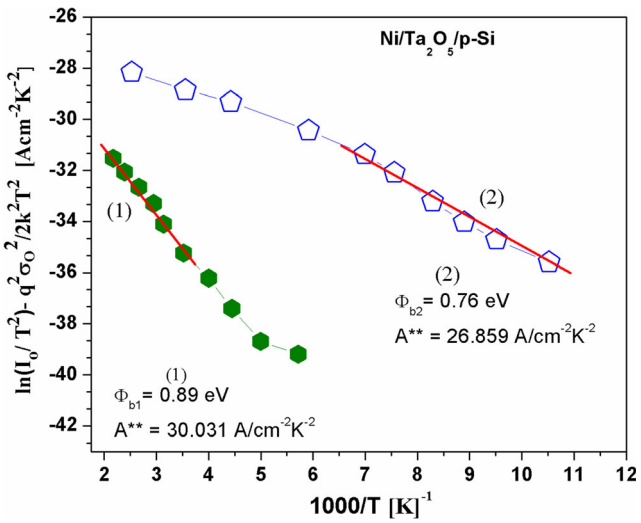

Fig. 9 $\ln(I_o/T^2)$-$q^2\sigma_0^2/2(kT)^2$ versus 1000/T plot for the for Ni/Ta_2O_5/p-Si SBD in the temperature regime 175–400 K

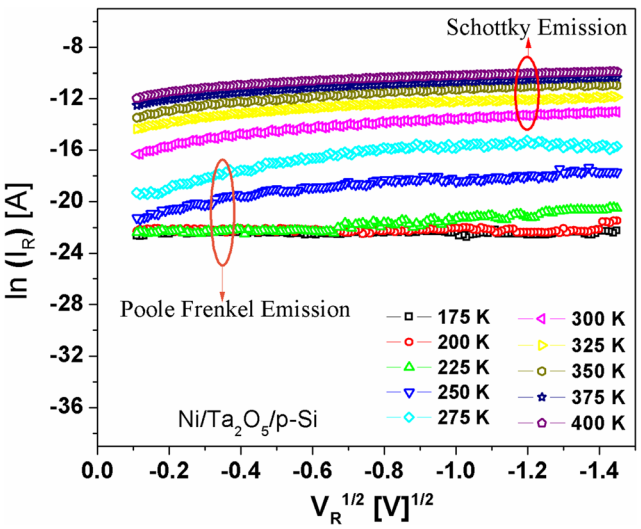

Fig. 10 Plot of $V_R^{1/2}$ versus $\ln(I_R)$ for Ni/Ta_2O_5/p-Si SBD in the temperature regime 175–400 K

that the experimental values determined in the low temperature regime (T < 275) were closer to the PFE lowering coefficient (β_{PE}), whereas the experimental values in the higher temperature regime (T > 300) were closer to the SFE lowering coefficient (β_{SE}). These results suggest that PFE is dominant in the lower temperature region while SE is dominant in the higher temperature region. Therefore, the current conduction mechanism of Ni/Ta_2O_5/p-Si MIS SBD switched from PFE to SE in the temperature regime of 300–400 K.

4 Conclusions

The electrical properties and carrier transport processes taking place in Ni/Ta_2O_5/p-Si MIS type SBDs were analysed in the temperature regime 175–400 K as a function of measurement temperature. Experimental results indicated that the diode parameters such as Φ_b, n and R_s were found to depend strongly on operating temperature. Double GD of the BH was evident from the plot of Φ_{bo} versus 1/2kT plot. The mean BHs 0.89 eV and 0.76 eV values extracted from modified Richardson plot are in well agreement with those (0.92 eV and 0.79 eV) obtained from Φ_{bo} versus 1/2kT plot. The extracted A* values 30.03 and 26.85 $A/cm^{-2} K^{-2}$ from modified Richardson plot is in well agreement with the theoretical value of 32.6 $A/cm^{-2} K^{-2}$ for p-type Si. Two types of current conduction mechanisms such as P-F emission (175–275 K) and SE (above 300 K) exists in Ni/Ta_2O_5/p-Si MIS SBDs, where the transition temperature for these two mechanisms was 275 K. In conclusion, the dependence of diode parameters on measurement temperature was successfully explained on account of double GD of BHs with the help of barrier inhomogeneities that prevail at the Ni/Ta_2O_5/p-Si junction.

Acknowledgements The author Dr. N. Nanda Kumar Reddy thankfully acknowledges the financial support received from the Department of Science and Technology (DST), Science and Engineering Research Board, Government of India, Major Research Project No. ECR/2017/002868, DST-FIST Program-2015 (SR/FST/College-263) and MITS/TEQIP-II/FACULTY-SEED GRANT/16-17/20 & 19-20.

Dr. Chandramohan Kukkambakam thankfully acknowledge the financial support from MRP Project No. 6395/16 (SERO/UGC), the University Grants Commission (UGC), Government of India.

References

1. Peercy PS (2000). Nature 406:1023
2. Manchanda L, Morris MD, Green ML, Dover RWV, Klemens F, Sorsch TW, Silverman PJ, Wilk G, Busch B, Aravamudhan S (2001). Microelctron Eng 59:351
3. Atanassova E, Konakova RV, Mitin VF, Koprinarova J, Lytvym OS, Okhrimenko OB, Schinkarenko VV, Virovska D (2005). Microelectron Reliab 45:123
4. Cappellani A, Keddie JL, Barradas NP, Jackson SM (1999). Solid State Electron 43:1095
5. Yu J, Chen G, Li CX, Shafiei M, Ou JZ, du Plessis J, Kalantar-Zadeh K, Lai PT, Wlodarski W (2011). Sens Actuators A 172:9
6. Moldovan M, Weyant CM, Johnson DL, Faber KT (2004). J Thermal Spray Tech 13:51
7. Chaneliere C, Autran JL, Devine RAB, Balland B (1998). Mater Sci Eng R-R 22:269
8. Tepehan FZ, Ghodsi FE, Ozer N, Tepehan GG (1999). Sol Energy Mater Sol 59:265
9. Ushikubo T (2000). Catal Today 57:331
10. Wolf MJ, Roitsch S, Mayer J, Nijmeijer A, Bouwmeester HJM (2013). Thin Solid Films 527:354
11. Boughaba S, Sproule GI, McCaffery JP, Islam M, Graham MJ (2000). Thin Solid Films 358:104
12. Demircioglu O, Karatas S, Yıldırım N, Bakkaloglu OF, Turut A (2011). J Alloys Compd 509:6433
13. Sharma M, Tripathi SK (2012). J Appl Phys 112:024521
14. Osiris WG, Farag AAM, Yahia IS (2011). Synth Met 161:1079
15. Gullu O, Aydogan S, Turut A (2012). Solid State Commun 152:38113
16. Deniz AR, Caldiran Z, Metin O, Meral K, Aydogan S (2016). J Colloid Interface Sci 473:172
17. Reddy VR, Reddy NNK (2012). Superlattice Microst 52:484
18. Reddy NNK, Reddy VR (2010). Opto Electron Adv Mater Rapid Commun 4:1229
19. Reddy NNK, Ananda P, Verma VK, Bakash KR (2019). Surf Rev Lett1950073. https://doi.org/10.1142/S0218625X19500732
20. Gozeh BA, Karabulut A, Yildiz A, Yakuphanoglu F (2018). J Alloys Comp 732:16
21. Ameen BAH, Yildiz A, Farooq WA, Yakuphanoglu F (2019). Silicon 11:563
22. Gozeh BA, Karabulut A, Yildiz A, Dere A, Arif B, Yakuphanoglu F (2019). Silicon. https://doi.org/10.1007/s12633-019-00266-7
23. Gozeh BA, Karabulut A, Ammen MM, Yildiz A, Yakuphanoglu F (2019) Surf Rev Lett. https://doi.org/10.1142/S0218625X19501737
24. Jang SH, Jang JS (2013). Electron Mater Lett 9:245
25. Cheung SK, Cheung NW (1986). Appl Phys Lett 49:85
26. Buyukbas Ulusan A, Tataroglu A, Azizian-Kalandaragh Y, Altındal S (2018). J Mater Sci Mater Electron 29:159
27. Kaymak N, Efil E, Seven E, Tataroglu A, Bilge S, Oz Orhan E (2019). Mater Res Express 6:026309
28. Kumar R, Chand S (2015). Electron Mater Lett 11:973
29. Kumar A, Kumar A, Sharma KK, Chand S (2019). Superlattice Microst 128:373
30. Norde H (1979). J Appl Phys 50:5052
31. Reddy NNK, Godavarthi S, Kumar KM, Kummara VK, Vattikuti SVP, Akkera HS, Bitla Y, Jilani SAK, Manjunath V (2019). J Mater Sci:Mater Electron 30:8955
32. Hamdaoui N, Ajjel R, Salem B, Gendry M (2014). Mater Sci Semicond Process 26:431
33. Aydogan S, Saglam M, Turut A, Onganer Y (2009). Mater Sci Eng C 29:1486
34. Reddy NNK, Reddy VR (2012). Bull Mater Sci 35:53
35. Ozdemir AF, Turut A, Kokce A (2006). Semicond Sci Technol 21:298
36. Reddy NNK, Akkera HS, Sekhar MC, Uthanna S (2019). Silicon 11:159
37. Ganichev SD, Ziemann E, Prettl W, Yassievich IN, Istratov AA, Weber ER (2000). Phys Rev B 61:10361
38. Padovani FA, Stratton R (1966). Solid State Electron 9:695

Publisher's Note Springer Nature remains neutral with regard to jurisdictional claims in published maps and institutional affiliations.